Joint Narrowband RFI Suppression and Phase Synchronization Signal Retrieval for BiSAR via Robust Principal Component Analysis

Yuesheng Chen, Yijiang Nan, Yonghua Cai, Pingping Lu, Robert Wang, *Senior Member, IEEE*

***Abstract*—Due to the complex electromagnetic environment and the increased demand for frequency occupation, radio frequency interference (RFI) is becoming a significant issue for the bistatic synthetic aperture radar (BiSAR), especially in the synchronization links. This paper proposes a novel rank prior matrix recovery (RPMR) method based on the robust principal component analysis (RPCA) to suppress the interferences in phase synchronization of BiSAR, by which the high-accuracy synchronization phase can be acquired. First, a signal model considering the RFI in phase synchronization is proposed, proving that the synchronization signal matrix and the RFI signal matrix have the low-rank and sparsity properties in the range frequency domain, respectively. Thus, the constraint conditions of RPCA can be satisfied. Then, the RPMR method is proposed to acquire the low-rank matrix representing the synchronization signal and the sparsity matrix representing the RFI signal. In RPMR, the partial singular value decomposition utilizing the rank prior is used to replace the traditional total singular value decomposition, thus reducing the computational cost. Finally, the high-accuracy synchronization phase can be extracted from the synchronization signal by the pulse compression. Simulation and experimental results using the real measured synchronization data of LuTan-1 (LT-1) validate the superiority of the proposed method.**

***Index Terms*—Radio frequency interference, bistatic synthetic aperture radar, phase synchronization, low-rank and sparsity recovery.**

I. Introduction

SYNTHETIC aperture radar (SAR) as a typical microwave remote sensing sensor has a unique capability in imaging, which can provide two-dimensional images in all day and all weather conditions, thus playing a significant role in the remote-sensing applications [1]–[4]. Compared with the monostatic SAR, bistatic synthetic aperture radar (BiSAR) with the separated transmitter and receiver has been a hot topic in recent years due to the many advantages, e.g., high-resolution wide-swath imaging, multi-baseline interferometric elevation measurement, and multi-angle observation [5]–[8]. However, an additional phase modulation generated by the different oscillators impacts the SAR imaging and interferometry, thus requiring phase synchronization to guarantee the coherence in SAR echoes. The non-interrupted synchronization scheme is an advanced method to achieve phase synchronization, which has been successfully implemented in the practical LuTan-1 (LT-1) [9]–[12].

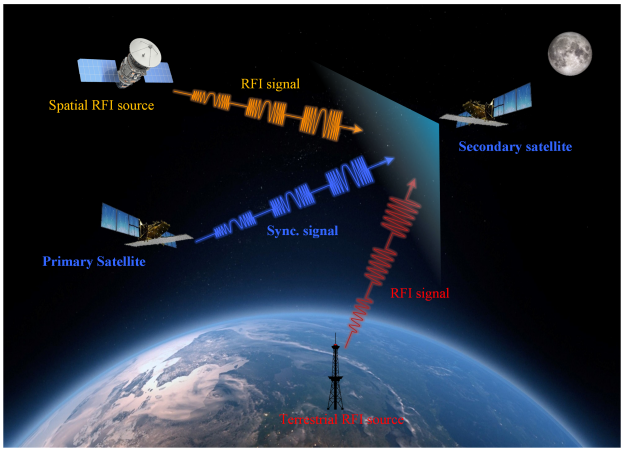

Fig. 1. Diagram of phase synchronization impacted by RFI.

In the LT-1 system, the phase synchronization links are easily impacted by the radio frequency interference (RFI) as shown in Fig. 1 due to the two reasons [13]. On one hand, the electromagnetic environment is becoming increasingly complicated with the advancement of navigation and wireless communication technology, leading to the scarcity of radio spectrum resources, especially in low-frequency bands. The phase synchronization links of LT-1 work in L-band, which conflicts with the navigation and communication radio spectrum due to the frequency allocation rules imposed by the International Telecommunications Union (ITU) [14], thus leading to the co-frequency contamination of the synchronization. On the other hand, the synchronization antennas equipped in LT-1 have wide beamwidth to achieve the omnidirectional communication in the non-interrupted synchronization scheme [7], thus increasing the possibility of receiving interference signals. The accuracy of phase synchronization is impacted by the RFI signals, degrading the BiSAR imaging and interferometry. To acquire the high-accuracy synchronization phase, the RFI mitigation is a key step in the processing of synchronization signals [13].

The existing RFI mitigation methods can be mainly categorized into three groups: parametric methods, nonparametric

Manuscript received XX XX, XXXX; revised XX XX, XXXX. This work was supported by the Chinese Academy of Science Key Project under Grant E33701010F. *(Corresponding author: Yijiang Nan.)*

Yuesheng Chen, Yijiang Nan, Yonghua Cai, Pingping Lu, and Robert Wang are with the National Key Laboratory of Microwave Imaging Technology, Aerospace Information Research Institute, Chinese Academy of Sciences, 100190, Beijing, China, and also with the School of Electronic, Electrical and Communication Engineering, University of Chinese Academy of Sciences, 100049, Beijing, China (e-mail: chenyuesheng21@mails.ucas.ac.cn; nanyj@aircas.ac.cn; caiyonghua19@mails.ucas.edu.cn; lupp@aircas.ac.cn; yuwang@mail.ie.ac.cn).

methods, and semiparametric methods [15]–[17]. The parametric methods, e.g., the parametric maximum likelihood (PML) [18] and least-squares estimation (LSE) [19], first reconstruct the narrowband interference signals (NBIs) by estimating the amplitude, frequency, and phase of the NBIs adaptively and then remove the reconstructed NBIs from the received signals. The performance of parametric methods is limited to the accuracy of the interference signal model. In addition, the parametric methods are not practical for non-stationary interferences due to the complicated signal model [14]. The nonparametric methods can separate the interferences and the useful signals, achieved by utilizing the time or frequency characteristics of the interference in the transforming domain [16]. Compared with the parametric methods, the nonparametric methods can suppress the interferences without establishing the complicated signal model, achieving better RFI mitigation results. Typical nonparametric methods include the frequency-domain notch filtering (FNF) [20] and eigen-subspace projection (ESP) [21]. The FNF method is suitable for suppressing the NBI, which is efficient and easy to achieve [20]. However, it causes the gapped spectrum inevitably, resulting in the worse SNR and degrading the RFI mitigation performance. In addition, the detection of RFI is also a challenge for FNF in practice [16]. The ESP method can successfully suppress the interferences in the case of strong RFI signals [21]. However, the computation cost of ESP is high. The semiparametric methods first formulate hyperparameter optimization problems by assuming certain conditions, e.g., the low-rank and sparsity properties [22], [23], and then solve them by convex optimization techniques [16], which have better RFI suppression performance even if the interferences are strong. However, the establishment of signal model characterized by the low-rank and sparsity properties is a significant challenge for these methods. In addition, high calculation cost are also required, thus leading to the inefficiency of semiparametric methods.

In this paper, a novel rank prior matrix recovery (RPMR) method based on robust principal component analysis (RPCA) is proposed to suppress the narrowband interferences in phase synchronization. We first propose a signal model with the range fast-time and azimuth slow-time contaminated by NBIs based on the non-interrupted phase synchronization scheme, and the low-rank property of the synchronization signal matrix and the sparsity property of the interference signal matrix in range frequency domain are proved using the proposed model respectively, thus satisfying the constraint conditions of RPCA. Then, the RPMR method using the partial singular value decomposition (P-SVD) is proposed to separate the synchronization signal and the narrowband interferences, by which the high-accuracy synchronization phase can be acquired with less computation cost. Finally, both simulation and experimental results using the real measured synchronization data of LT-1 have been conducted to validate the superior RFI mitigation performance of the proposed method. The main contributions of this article are listed as follows:

1) A 2-D signal model contaminated by the NBIs in phase synchronization is presented for the first time.

2) The low-rank and sparsity property of signal matrices in range frequency domain are proved.

3) A novel rank prior matrix recovery method is proposed to suppress the NBIs in phase synchronization.

This paper is organized as follows. In Section II, the signal model based on the non-interrupted phase synchronization scheme is first introduced, and the characteristics of the synchronization signal and NBIs are analyzed. Then, the RPMR method for RFI mitigation in phase synchronization is proposed in Section III. The simulation and experimental results based on LT-1 are presented in Section IV. Finally, conclusions are drawn in Section V.

II. Signal Model and Characteristics

In this section, we first introduce the signal model with the range fast-time and azimuth slow-time based on the non-interrupted phase synchronization scheme. Then, the low-rank property of the synchronization signal matrix and the sparsity properties of the interference signal matrix are proved, respectively.

A. Signal Model

In the non-interrupted phase synchronization scheme, the received data contaminated by RFI can be modeled as [14]

$$R(\tau,t)=S(\tau,t)+I(\tau,t)+N(\tau,t) \tag{1}$$

where $S(\tau,t)$, $I(\tau,t)$ and $N(\tau,t)$ are the synchronization signal, interference signals and noise, respectively. τ and t are the range-fast time and azimuth-slow time respectively.

The synchronization signal transmitted by the primary satellite is received by the secondary satellite frame by frame along with the azimuth-slow time, which can be modeled as a 2-D matrix:

$$\begin{aligned} S(\tau,t)=&\operatorname{rect}\left\{\frac{\tau-\tau_{\text{ab}}}{T_{\text{syn}}}\right\}\exp\left\{j\pi K_{\text{syn}}(\tau-\tau_{\text{ab}})^2\right\}\\ &\times\exp\left\{-j2\pi f_T\tau_{\text{ab}}\right\}\exp\left\{j\varphi(t)\right\}\exp\left\{jn(t)\right\}\end{aligned} \tag{2}$$

where T_{syn}, K_{syn}, τ_{ab}, and f_T are the pulse width, chirp rate, time delay, and carrier frequency of the transmitter, respectively. The time-varying phase $\varphi(t)$ can be expressed as [11], [24]

$$\varphi(t)=\pi(f_R-f_T)t+\phi_R(t) \tag{3}$$

where f_R is the carrier frequency of the receiver, and $\phi_R(t)$ can be considered as a constant phase in a short time. The oscillator phase noise $n(t)$ can be expressed as [24]

$$n(t)=\theta_T(t-\tau_{\text{ab}})-\theta_R(t) \tag{4}$$

where $\theta_T(t)$ and $\theta_R(t)$ are the transmitter phase noise and the receiver phase noise respectively, which can be modeled by a second-order stationary stochastic process. The power spectral density $S_\phi(f)$ of the process can be expressed as [25], [26]

$$S_\phi(f)=af^{-4}+bf^{-3}+cf^{-2}+df^{-1}+e \tag{5}$$

where the coefficients $a-e$ are contributions from 1) random walk frequency noise, 2) flicker frequency noise, 3) white frequency noise, 4) flicker phase noise, and 5) white phase noise, respectively [11]. The typical coefficients $a-e$ is shown

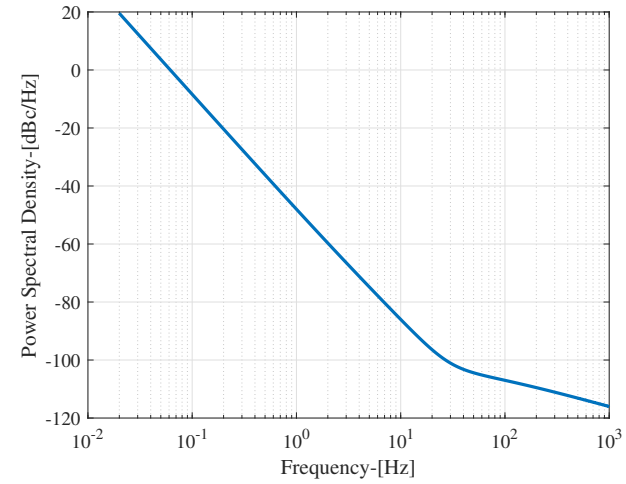

(a)

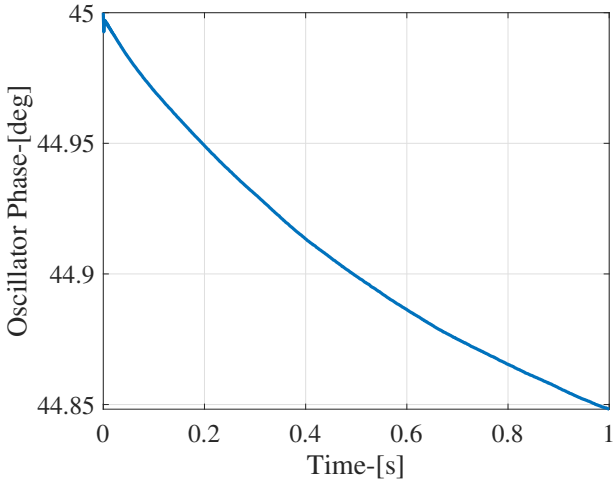

(b)

Fig. 2. Oscillator phase noise of LT-1. (a) The power spectrum of the oscillator of LT-1. (b) The oscillator phase noise in a short time.

TABLE I: Typical coefficients of a oscillator.

a	b	c	d	e
-48 dB	-58 dB	-71 dB	-85 dB	-168 dB

in Table I. The phase spectrum $S_\phi(f)$ and phase noise of the oscillator are shown in Fig. 2. It can be seen that the oscillator phase noise is very small when the azimuth time is short. Therefore, the oscillator phase noise can be ignored in a short azimuth time, and the synchronization signal model can be approximately expressed as

$$\begin{aligned} S(\tau,t) = &\text{rect}\left\{\frac{\tau-\tau_{\text{ab}}}{T_{\text{syn}}}\right\}\exp\left\{j\pi K_{\text{syn}}(\tau-\tau_{\text{ab}})^2\right\} \\ &\times\exp\left\{-j2\pi f_T\tau_{\text{ab}}\right\}\exp\left\{j\pi\left(f_R-f_T\right)t+\phi_R\right\} \end{aligned} \tag{6}$$

The interference signals in phase synchronization mainly come from the radiation sources operating in the same frequency band as the BiSAR system, including the spaceborne sources, e.g., co-frequency communication satellite and terrestrial sources, e.g., commercial land-mobile radio [14]. The interferences transmitted by these sources and the synchronization signal transmitted by primary satellite may be received by the secondary satellite simultaneously in the BiSAR system shown in Fig. 1, thus degrading the accuracy of phase synchronization. From the measured synchronization data of LT-1 shown in Fig. 3, the RFIs in phase synchronization are usually narrowband interference signals. Based on the narrowband characteristics, the NBIs are assumed to a sum of multiple complex sinusoids, which can be modeled as

$$I(\tau,t)=\sum_{m=1}^{M}A_m(t)\exp\left\{j2\pi f_m(t)\tau+j\theta_m(t)\right\} \tag{7}$$

where $A_m(t)$, $f_m(t)$ and $\theta_m(t)$ represent the amplitude, frequency, and phase of the m-th component respectively, and M is the number of RFI signals.

B. Properties of Signal Matrices

Based on the signal model, the low-rank property of the synchronization signal matrix and the sparsity property of the NBIs matrix are proved respectively.

1) *Low-rank Property*: The synchronization signals with the same waveform transmitted by the primary satellite are received by the secondary satellite, and these synchronization signals only differ in phase. From Eq. (6), the range-frequency-domain expression of the synchronization signal matrix can be derived using the principle of stationary phase (POSP):

$$\begin{aligned} \mathbf{S}_f &= \text{FFT}\left\{S(\tau,t)\right\} \\ &= \text{rect}\left\{\frac{f_\tau}{K_{\text{syn}}T_{\text{syn}}}\right\}\exp\left\{-j\pi\frac{f_\tau^2}{K_{\text{syn}}}\right\} \\ &\times\exp\left\{-j2\pi f_\tau\tau_{\text{ab}}\right\}\exp\left\{-j2\pi f_T\tau_{\text{ab}}\right\}\exp\left\{j\varphi(t)\right\} \end{aligned} \tag{8}$$

where f_τ is the range frequency. Obviously, there is only a linear phase difference $\varphi(t)$ between frames in range frequency domain. Therefore, the synchronization signal matrix in range frequency domain has the low-rank property, and its rank is one.

To validate the low-rank property, the real measured synchronization data of LT-1 are analyzed. The singular value curve of the data are presented in Fig. 4(a). Note that there is only one lager singular value, demonstrating the low-rank property of the synchronization signal matrix.

2) *Sparse Property*: From Eq. (7), the range-frequency-domain expression of the NBIs matrix can be derived as

$$\begin{aligned} \mathbf{I}_f &= \text{FFT}\left\{I(f_\tau,t)\right\} \\ &= \sum_{m=1}^{M}2\pi A_m(t)\exp\left\{j\theta_m(t)\right\}\delta\left(f_\tau-f_m(t)\right) \end{aligned} \tag{9}$$

where $\delta(\cdot)$ is Dirac function. It can be seen that the frequency of NBIs only occupies a single frequency point due to the narrowband characteristic, thus leading to the sparsity in range frequency domain. From the measured synchronization data shown in Fig. 3, the energy of NBIs is concentrated at a

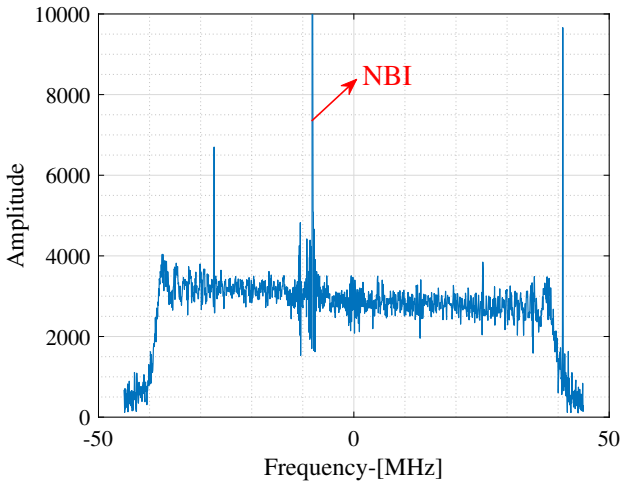

(a)

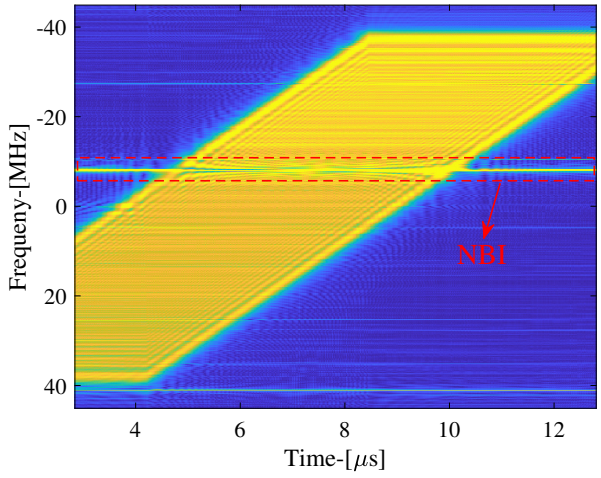

(b)

Fig. 3. Real measured synchronization data of LT-1. (a) Spectrum of the contaminated synchronization signal. (b) Time-frequency diagram of the contaminated synchronization signal.

specific frequency, not the whole frequency axis, validating the sparsity of NBIs. To quantify the sparsity, S_p is defined as

$$S_p = \frac{Z_0}{Z_{\text{total}}} \tag{10}$$

where Z_0 and Z_{total} are the number of zero and total number in the quantization data matrix.

The sparsity of NBIs matrix is presented in Fig. 4(b) using the contaminated synchronization data of LT-1, which can be seen that the sparsity of NBIs matrix can reach 99.76%. It is evident that the NBIs matrix has high sparsity in range frequency domain.

III. NBIs SUPPRESSION METHOD

To suppress the NBIs in phase synchronization, a novel rank prior matrix recovery (RPMR) method based on RPCA is proposed in this section. We first review the RPCA technique briefly and then propose the RPMR method using the partial singular value decomposition (P-SVD) by which the high-accuracy synchronization phase can be acquired with less computation cost.

TABLE II: Synchronization parameters of the LT-1 system

Parameters	Values
Carrier frequency (F_0)	1.26 GHz
Pulse duration (T_{syn})	10 μs
Bandwidth (B_{syn})	80 MHz
Sampling frequency (F_{syn})	90 MHz
Chirp rate (K_{syn})	-8 MHz/μs

A. Robust Principal Component Analysis

The robust principal component analysis (RPCA) is the classical method to solve the problem of low-rank and sparsity matrix recovery, which interprets the observed data matrix as the superposition of a low-rank matrix and a sparsity matrix. The model of RPCA can be expressed as [27]–[29]

$$\mathbf{B} = \mathbf{L} + \mathbf{X} + \mathbf{N} \tag{11}$$

where $\mathbf{B}$, $\mathbf{L}$, $\mathbf{X}$, and $\mathbf{N}$ are the observed data matrix, low-rank matrix, sparsity matrix, and noise, respectively. To acquire the low-rank and sparsity matrices, the optimization problem with ℓ_1-norm regularization can be formulated as [30]

$$\begin{aligned} &\min_{\mathbf{L},\mathbf{X}} \ (\|\mathbf{L}\|_* + \lambda\|\mathbf{X}\|_1) \\ &\text{s.t.} \quad \|\mathbf{B}-\mathbf{L}-\mathbf{X}\|_F^2 < \delta \end{aligned} \tag{12}$$

where $\|\cdot\|_1$, $\|\cdot\|_*$, and $\|\cdot\|_F$ denote the ℓ_1 norm, nuclear norm, and Frobenius norm, respectively. δ and λ are the power level of noise and weight factor. Obviously, Eq. (12) is a convex optimization problem, which can be solved by the inexact augmented Lagrange multiplier (IALM) algorithm effectively [30]. The IALM algorithm uses the singular value decomposition and soft-thresholding to perform twice univariate optimization, which has better convergence and faster convergence speed.

Based on the low-rank and sparsity properties of the signal matrices discussed in Section II, the signal model in (1) satisfies the constraint conditions of RPCA in (11). Therefore, the RPCA can be used to suppress the NBIs in phase synchronization.

B. Proposed Method

The key points of the proposed RPMR method are the matrix recovery based on the RPCA in range frequency domain and the partial singular value decomposition (P-SVD) utilizing the rank prior. The specific processing flow is summarized in Algorithm 1.

First, the received data are arranged into a 2-D matrix and transformed into the range frequency domain expressed as

$$\mathbf{R}_f = \text{FFT}_\tau\left\{R(\tau,t)\right\} \tag{13}$$

where $\text{FFT}_\tau\{\cdot\}$ and $\mathbf{R}_f$ are the range Fourier transform and range-frequency matrix.

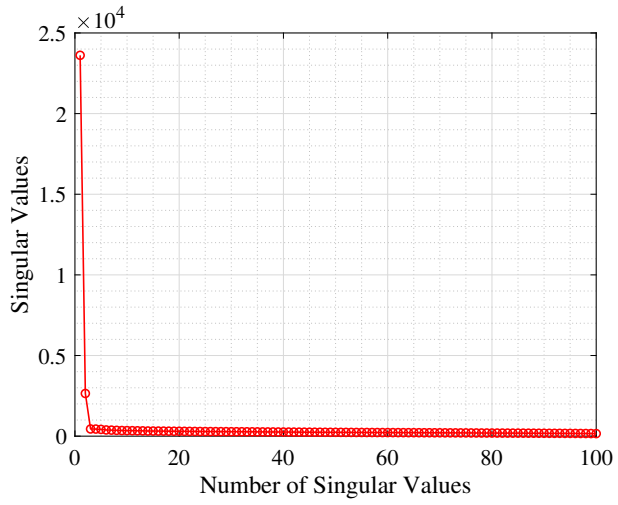

(a)

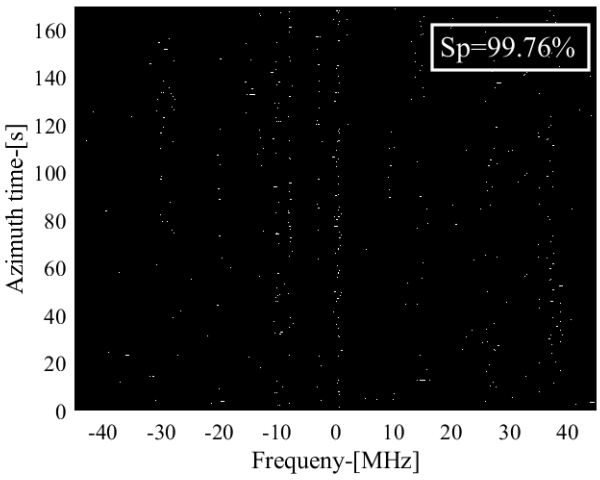

(b)

Fig. 4. Characteristics of signal matrices. (a) Low-rank property of the synchronization signal matrix. (b) Sparsity property of NBIs matrix.

Then, the IALM algorithm is used in range frequency domain to achieve the matrix recovery. The augmented Lagrange function can be written as [27], [30]

$$G\left(\mathbf{S}_f,\mathbf{I}_f,\mathbf{Y},\mu\right)=\|\mathbf{S}_f\|_*+\lambda\|\mathbf{I}_f\|_1+\langle\mathbf{Y},\mathbf{R}_f-\mathbf{S}_f-\mathbf{I}_f\rangle+\frac{\mu}{2}\|\mathbf{R}_f-\mathbf{S}_f-\mathbf{I}_f\|_F^2 \tag{14}$$

where μ is a penalty factor. Given the initial value $\mathbf{S}_f^0$, $\mathbf{I}_f^0$, $\mathbf{Y}_0$, and μ_0, the optimal solution can be obtained through the alternate univariate optimization, which can be derived as [15], [29]

$$\begin{aligned}\mathbf{S}_f^{k+1}&=\arg\min_{\mathbf{S}_f}\left\{G\left(\mathbf{S}_f,\mathbf{I}_f^{k+1},\mathbf{Y}_k,\mu_k\right)\right\}\\&=D_{1/\mu_k}\left(\mathbf{R}_f-\mathbf{I}_f^{k+1}+\frac{\mathbf{Y}_k}{\mu_k}\right)\end{aligned} \tag{15}$$

Algorithm 1 Rank Prior Matrix Recovery

Input:

a) $R\left(\tau,t\right)\in\mathbb{C}^{M\times N}$, Raw data matrix.
b) λ, weight factor.
c) μ, penalty factor.
d) ρ, learning rate.
e) ε, error tolerance.
f) K, maximum number of iterations.

Output:

$\hat{S}\left(\tau,t\right)$, the synchronization signal matrix after RFI suppression.
$\hat{I}\left(\tau,t\right)$, the interference signal matrix.

Transform $R\left(\tau,t\right)$ into the range-frequency domain: $\mathbf{R}_f=\mathrm{FFT}_\tau\left\{R\left(\tau,t\right)\right\}$.
Initialize $\mathbf{S}_f^0=\mathbf{0}$, $\mathbf{I}_f^0=\mathbf{0}$, $\mathbf{Y}_0=\mathbf{0}$, and $\mu_0=\sqrt{\max\left\{M,N\right\}}$.
for $k=1$ to K **do**
  Given $\mathbf{I}_f^k=\mathbf{0}$, $\mathbf{Y}_k$, and μ_k, optimize the $\mathbf{S}_f^k$: $\mathbf{S}_f^{k+1}=D_{1/\mu_k}\left(\mathbf{R}_f-\mathbf{I}_f^{k+1}+\frac{\mathbf{Y}_k}{\mu_k}\right)$.
  Given $\mathbf{S}_f^{k+1}=\mathbf{0}$, $\mathbf{Y}_k$, and μ_k, optimize the $\mathbf{I}_f^{k+1}$: $\mathbf{I}_f^{k+1}=F_{\lambda/\mu_k}\left(\mathbf{R}_f-\mathbf{S}_f^{k+1}+\frac{\mathbf{Y}_k}{\mu_k}\right)$.
  Update $\mathbf{Y}_k$: $\mathbf{Y}_{k+1}=\mathbf{Y}_k+\mu_k\left(\mathbf{R}_f-\mathbf{S}_f^{k+1}-\mathbf{I}_f^{k+1}\right)$.
  Update μ_k: $\mu_{k+1}=\min\left\{\rho\mu_k,\mu_{\max}\right\}$.
  Until $\left\|\mathbf{R}_f-\mathbf{S}_f^{k+1}-\mathbf{I}_f^{k+1}\right\|_F/\|\mathbf{R}_f\|_F<\varepsilon$.
end for
Transform $\mathbf{S}_f^*$ into the time domain: $\hat{S}\left(\tau,t\right)=\mathrm{IFFT}_\tau\left\{\mathbf{S}_f^*\right\}$
Return the synchronization signal matrix after RFI suppression: $\hat{S}\left(\tau,t\right)$

$$\begin{aligned}\mathbf{I}_f^{k+1}&=\arg\min_{\mathbf{I}_f}\left\{G\left(\mathbf{S}_f^{k+1},\mathbf{I}_f,\mathbf{Y}_k,\mu_k\right)\right\}\\&=F_{\lambda/\mu_k}\left(\mathbf{R}_f-\mathbf{S}_f^{k+1}+\frac{\mathbf{Y}_k}{\mu_k}\right)\end{aligned} \tag{16}$$

$$\mathbf{Y}_{k+1}=\mathbf{Y}_k+\mu_k\left(\mathbf{R}_f-\mathbf{S}_f^{k+1}-\mathbf{I}_f^{k+1}\right) \tag{17}$$

$$\mu_{k+1}=\min\left\{\rho\mu_k,\mu_{\max}\right\} \tag{18}$$

where k, ρ, $\mu_{\max}$, $D_{1/\mu_k}\left(\cdot\right)$, and $F_{\lambda/\mu_k}\left(\cdot\right)$ are the iterations, learning rate, threshold of penalty factor, singular value thresholding operator, and soft thresholding operator, respectively.

Based on the signal matrix properties in Section III.A, the rank of the synchronization signal matrix is approximately one. Therefore, the RPMR method can utilize the partial singular value decomposition (P-SVD) to speed up the traditional IALM algorithm which uses the total singular value decomposition (T-SVD). The singular value thresholding operator using the P-SVD in the RPMR method can be derived as [30]

$$\left[\mathbf{U},\mathbf{D},\mathbf{V}\right]=\mathrm{psvd}\left\{\mathbf{Q},n\right\} \tag{19}$$

$$\mathbf{D}_o=\mathrm{sgn}\left(\mathbf{D}\right)\max\left(\mathrm{abs}\left(\mathbf{D}\right)-\alpha,0\right) \tag{20}$$

$$D_{\text{fast}}\left(\mathbf{Q}\right)=\mathbf{U}\mathbf{D}_o\mathbf{V}^H \tag{21}$$

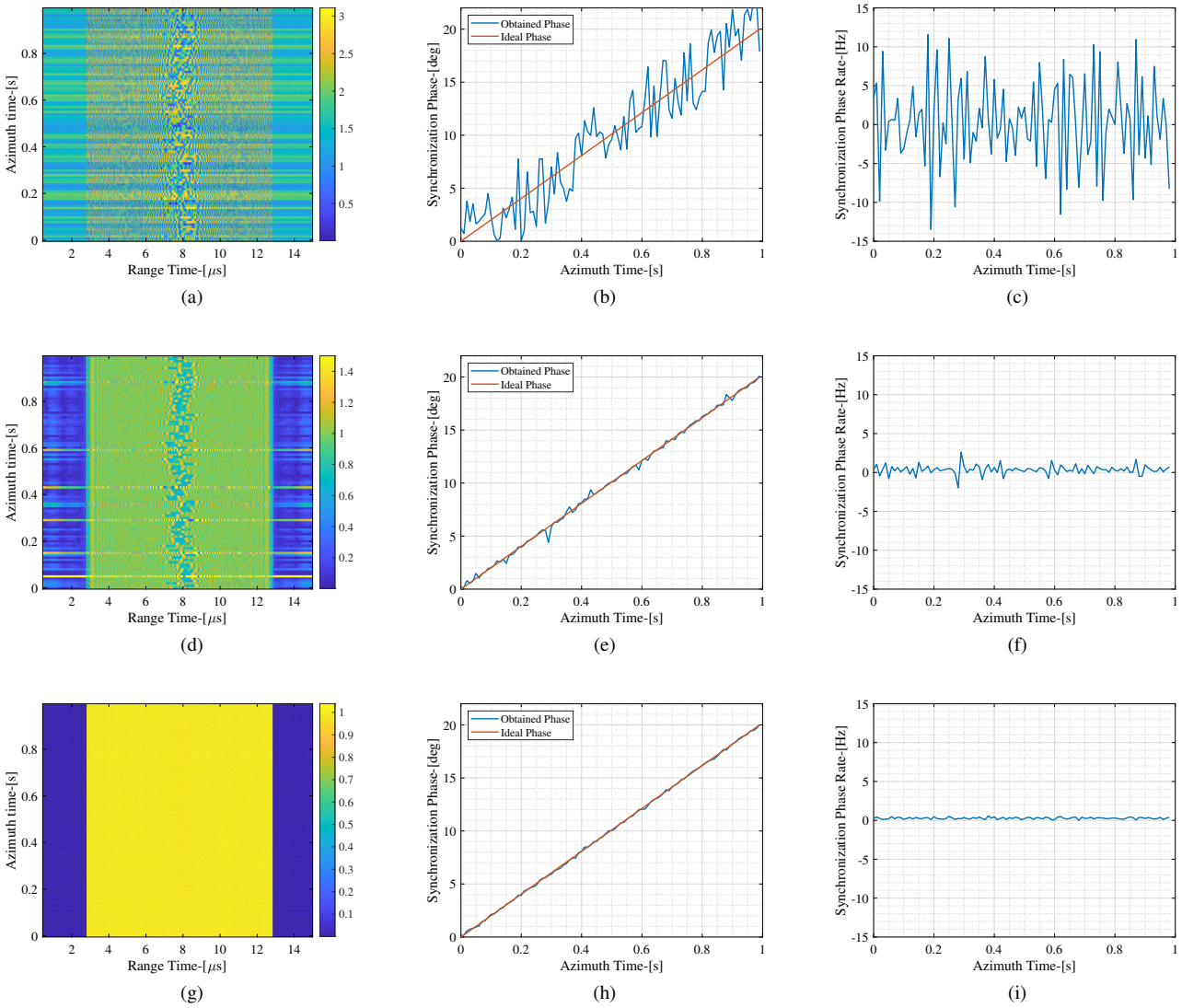

Fig. 5. RFI suppression results. (a∼c) the results without RFI suppression, where (a) is the amplitude of the synchronization data, (b) is the comparison between the obtained synchronization phase and the ideal synchronization phase, and (c) is the synchronization phase rate; (d∼f) the results with FNF method, where (d) is the amplitude of the synchronization data, (e) is the comparison between the obtained synchronization phase and the ideal synchronization phase, and (f) is the synchronization phase rate; (g∼i) the results with RPMR method, where (g) is the amplitude of the synchronization data, (h) is the comparison between the obtained synchronization phase and the ideal synchronization phase, and (i) is the synchronization phase rate.

where $\mathbf{U}$, $\mathbf{D}$, $\mathbf{V}$, $\mathbf{Q}$ and $\{\cdot\}^H$ are the matrix composed of left singular vectors, diagonal matrix composed of eigenvalues, matrix composed of right singular vectors, input matrix, and complex conjugate transpose, respectively. $\mathrm{psvd}(\cdot, n)$, $\mathrm{sgn}(\cdot)$, and $\mathrm{abs}(\cdot)$ represent the partial singular value decomposition acquiring the n largest singular values, signum function, and magnitude function, respectively. After matrix recovery using the proposed method, the optimal low-rank matrix $\mathbf{S}_f^*$ and sparse matrix $\mathbf{I}_f^*$ can be acquired.

Finally, the optimal low-rank signal matrix $\mathbf{S}_f^*$ is transformed into the time domain to achieve the RFI suppression, which can be derived as

$$\hat{S}(\tau, t) = \mathrm{IFFT}_\tau\left\{\mathbf{S}_f^*\right\} \tag{22}$$

where $\mathrm{IFFT}_\tau\{\cdot\}$ and $\hat{S}(\tau, t)$ are the range inverse Fourier transform and synchronization signal matrix after RFI suppression, respectively. The high-accuracy synchronization phase can be obtained by pulse compression of $\hat{S}(\tau, t)$. The proposed method is summarized as follows.

Step 1: Arrange the received data into a 2-D matrix, and then transform the 2-D matrix into the range frequency domain.

Step 2: Apply the RPMR method to the frequency-domain matrix $\mathbf{R}_f$ to acquire the synchronization signal matrix without RFI.

Step 3: Transform the synchronization signal matrix into the time domain, and then perform pulse compression to obtain the high-accuracy synchronization phase.

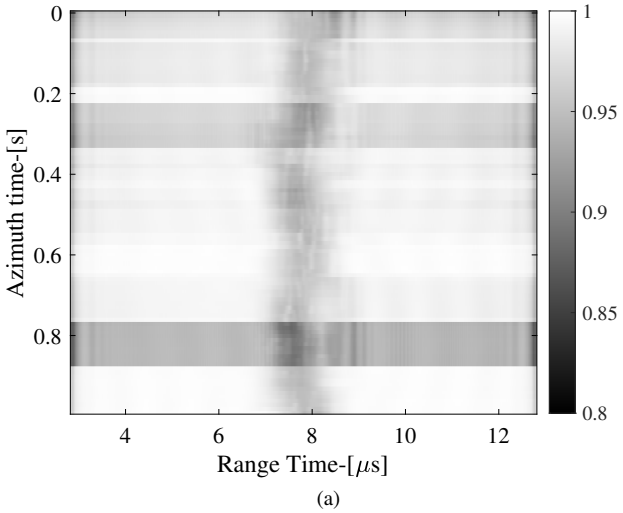

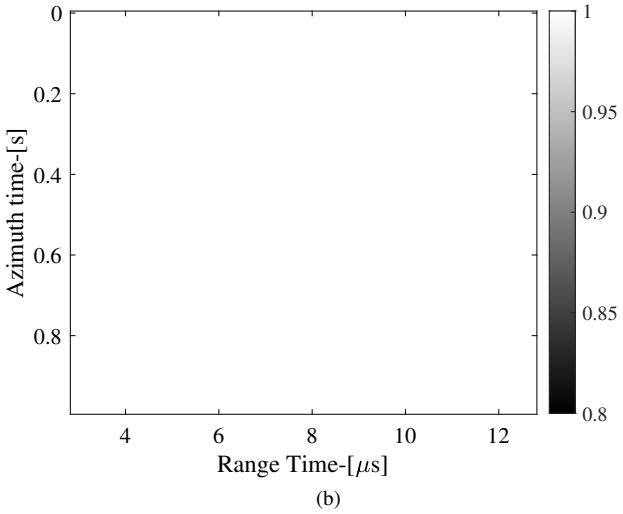

Fig. 6. Coherence diagram between the reference signal matrix and the processed signal matrix. (a) Processed by FNF. (b) Processed by RPMR.

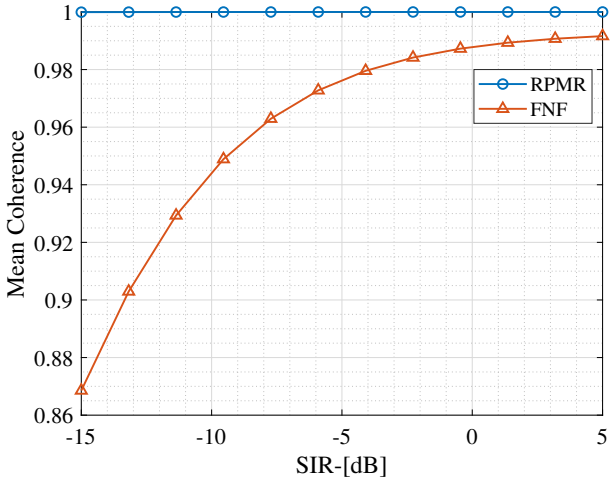

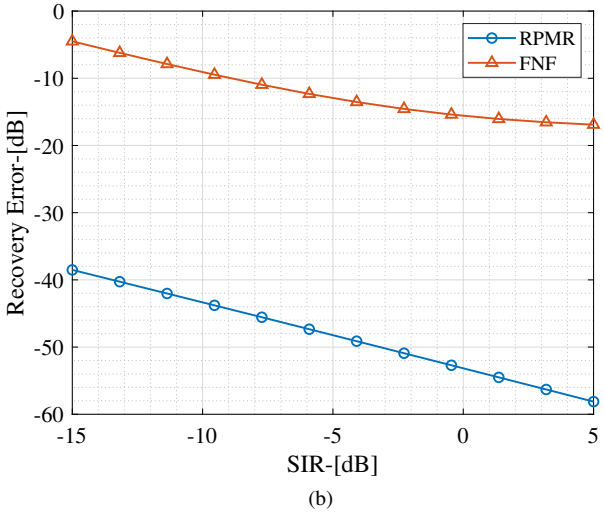

Fig. 7. SIR performance investigation. (a) mean coherence. (b) recovery error.

IV. Experimental Results

To demonstrate the effectiveness of the proposed RPMR method, both the simulated data based on the synchronization parameters of LT-1 and real measured synchronization data of LT-1 are conducted in this section.

A. Simulation Results

The simulation is conducted based on the synchronization parameters of LT-1 listed in Table II. For simplicity, 100 frames of synchronization signals contaminated by the NBIs of different frequencies and phases are generated in the simulation. The parameters of NBIs are summarized in Table III. The white Gaussian noise is added to the simulated data, generating the noised signal with the signal-to-noise ratio (SNR) of 20dB. To present the performance of RFI mitigation methods clearly, the derivatives of phase versus azimuth time, i.e., synchronization phase rate, is defined as

$$F_{\text{syn}} = \frac{\phi(t)}{t} \tag{23}$$

where $\phi(t)$ is the obtained synchronization phase. The ideal synchronization phase rate is a constant due to the domination of the linear term from Eq. (6). The amplitude of the synchronization data is presented in Fig. 5(a). It can be seen that the data are polluted by the NBIs seriously, thus leading to the significant deviation of the synchronization phase shown in Figs. 5(b). The synchronization phase rate shown in Fig. 5(c) presents many jitters, illustrating the large synchronization phase error. The RFI mitigation results using the FNF method are presented in Figs. 5(d∼f). It can be seen from Fig. 5(d) that the NBIs are suppressed partially. However, some significant residual interferences still exist in the synchronization data due to the false detection of the interferences. In addition, the severe synchronization signal loss results in the worse SNR,

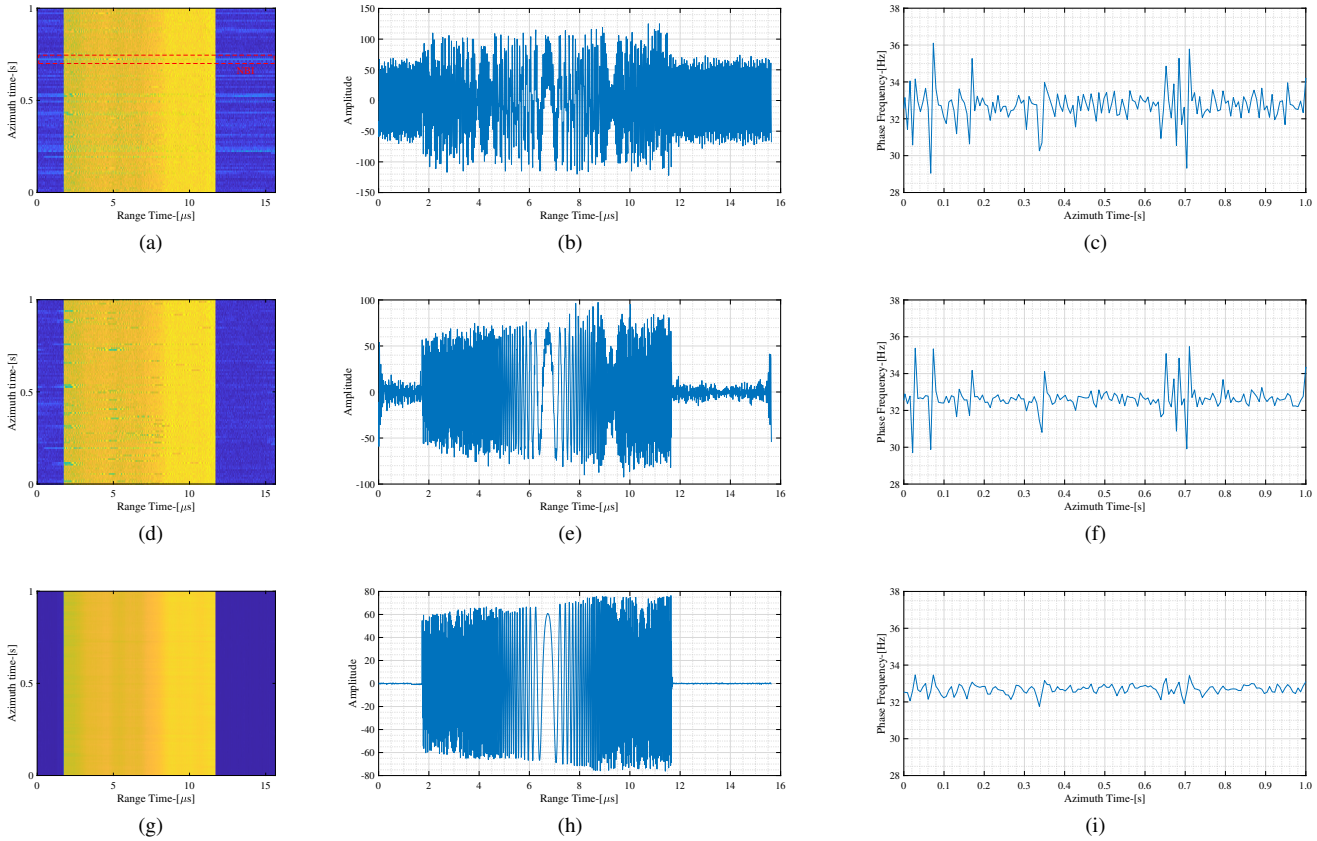

Fig. 8. The RFI mitigation results with the measured synchronization data of LT-1. (a∼c) the received data without RFI mitigation, where (a) is the 2-D synchronization signal matrix, (b) is the real part of one frame synchronization signal contaminated by RFI, and (c) is the obtained synchronization phase; (d∼f) the RFI mitigation results with FNF, where (d) is the 2-D synchronization signal matrix, (e) is the real part of one frame synchronization signal contaminated by RFI, and (f) is the obtained synchronization phase; (g∼i) the RFI mitigation results with RPMR, where (g) is the 2-D synchronization signal matrix, (h) is the real part of one frame synchronization signal contaminated by RFI, and (i) is the obtained synchronization phase.

TABLE III: Interference parameters setting

Parameters	**Values**
Carrier frequency (F_j)	1.26 GHz $\pm$ 5 MHz
Initial phase (ϕ_j)	10°-100°
Number of RFI frames	100

degrading the performance of the FNF method significantly. The RFI mitigation results using the proposed RPMR method are presented in Figs. 5(g∼i). Compared with the FNF method, most NBIs are suppressed as shown in Fig. 5(g), and the deviation between the obtained synchronization phase and the ideal synchronization phase is very small shown in Fig. 5(h). In addition, the obtained synchronization phase rate shown in Fig. 5(i) is approximately a constant compared with that of the FNF, demonstrating the better performance of the proposed method.

To evaluate the phase consistence, the coherence between the ideal and processed synchronization signal matrix are calculated, which is defined as [31]

$$\mathbf{C} = \frac{\left| E\left\{\hat{\mathbf{S}}\mathbf{S}^*\right\}\right|}{\sqrt{E\left\{\left\|\hat{\mathbf{S}}\right\|_2^2\right\} E\left\{\|\mathbf{S}\|_2^2\right\}}} \tag{24}$$

where $\hat{\mathbf{S}}$ and $\mathbf{S}$ are the processed and ideal synchronization signal matrix respectively. $E\{\cdot\}$, $\{\cdot\}^*$ and $\|\cdot\|_2$ are the expectation operator, conjugate operator and ℓ_2 norm, respectively. The coherence results are shown in Fig. 6. The Black represents the low coherence, and the white represents the high coherence. Obviously, the coherence of the RPMR method is much higher than that of the FNF method, demonstrating the better phase consistence of the proposed method.

To further validate the robustness of the proposed method, the signal-to-interference ratio (SIR) of the proposed method is investigated. The NBI signals with the SIR from -15dB to 5dB are generated. The mean coherence and recovery error are used to evaluate the robustness of the proposed method.

TABLE IV: Statistical results of synchronization phase rate

Methods	Mean (Hz)	STD (Hz)	COV
Without RFI Mitigation	32.7320	0.7935	0.0242
RFI Mitigation by FNF	32.7312	0.7069	0.0216
RFI Mitigation by RPMR	**32.6728**	**0.3861**	**0.0118**

The recovery error is defined as [31]

$$R = 10\log_{10}\left(\frac{\left\|\hat{\mathbf{S}}-\mathbf{S}\right\|_F^2}{\|\mathbf{S}\|_F^2}\right) \tag{25}$$

The simulation results are shown in Fig. 7. It can be seen that the mean coherence of the FNF method reduces as the interference energy increases. By comparison, the mean coherence of RPMR is quite high (≈ 1) and not be affected by the interferences. The recovery error of the RPMR method is quite smaller (< -35dB) than that of the FNF method, validating the better robustness of RPMR.

B. Experimental results of LuTan-1 synchronization data

The proposed method is verified using the real measured synchronization data of LT-1 in this subsection. The synchronization data are acquired by LT-1B on August 30, 2022, whose amplitude is shown in Fig. 8(a). It can be seen that many bright lines exist in the amplitude figure, which denote the NBI signals. To present the impact of the NBIs on the synchronization signal clearly, the real part of one frame synchronization signal is shown in Fig. 8(b). Obviously, the synchronization signal is distorted, demonstrating the serious contamination in phase synchronization. The obtained synchronization phase rate is shown in Fig. 8(c). Many jitters existing in the figure illustrate the large synchronization phase errors caused by the NBIs. The RFI suppression results using the FNF and the proposed RPMR are presented in Figs. 8(d)-(f) and Figs. 8(g)-(i), respectively. Compared with the FNF method, most NBIs are eliminated, and the better synchronization signal is recovered with less signal loss using the RPMR method. In addition, the obtained synchronization phase rate shown in Fig. 8(i) is closer to a constant, validating the performance of the proposed method for the real measured data.

To evaluate the performance of RFI mitigation quantitatively, the standard deviation (STD) and coefficient of variation (COV) are calculated. The statistical results of the synchronization phase rate are presented in Table IV. The STD and COV are quite large without RFI mitigation, illustrating the low accuracy of phase synchronization. The STD becomes smaller after the RFI mitigation using the FNF method. However, the COV remains virtually unchanged, not satisfying the requirements of high-accuracy phase synchronization. The STD and COV of the RPMR method are smallest in Table IV, thus demonstrating the superior RFI mitigation performance of the proposed method.

V. Discussion

The high-accuracy phase synchronization improves the quality of BiSAR images and the accuracy of the global digital elevation model (DEM), which is significant for the BiSAR system. However, the NBI signals impact the extraction of the synchronization phase, degrading the synchronization accuracy. To address this issue, we analyze the properties of the interference and synchronization signals in detail and propose an effective NBI suppression method. The proposed method can separate the NBIs and synchronization signals with less signal loss utilizing the sparse and low-rank recovery. However, the rank of the interference matrix increases as the bandwidth of interferences increases, deteriorating the low-rank property significantly. The performance of the proposed method degrades accordingly. To mitigate the wideband interferences (WBIs) better, we are considering structuring the advanced anti-interference system and using the new signal separation algorithm. For example, the multichannel phase synchronization system and blind source separation (BSS) algorithm provide a new processing framework.

VI. Conclusion

To acquire the high-accuracy synchronization phase, a novel rank prior matrix recovery method is proposed in this paper. First, we establish a signal model based on the non-interrupted synchronization scheme and prove the low-rank and sparsity properties of the signal matrices in range frequency domain. Then, the RPMR method is proposed to separate the synchronization signal and the interferences with less signal loss, in which the partial singular value decomposition is used based on the rank prior. Finally, the simulation and experimental results validate the performance of the proposed method. The work in this paper provides an effective method to suppress the NBIs in phase synchronization, which can be used in the processing of synchronization signals in the practical BiSAR system LT-1. However, the proposed method cannot be suitable for wideband interference signals, limiting the wide application of the proposed method. In future work, we will focus on the RFI suppression for the wideband interference.

References

[1] A. Moreira, P. Prats-Iraola, M. Younis, G. Krieger, I. Hajnsek, and K. P. Papathanassiou, "A tutorial on synthetic aperture radar," *IEEE Geoscience and Remote Sensing Magazine*, vol. 1, no. 1, pp. 6–43, 2013.

[2] M. Rodriguez-Cassola, S. V. Baumgartner, G. Krieger, and A. Moreira, "Bistatic TerraSAR-X/F-SAR spaceborne–airborne SAR experiment: Description, data processing, and results," *IEEE Transactions on Geoscience and Remote Sensing*, vol. 48, no. 2, pp. 781–794, 2010.

[3] Y. Zhang, S. Han, T. Wei, W. Wang, Y. Deng, G. Jin, Y. Zhang, and R. Wang, "First demonstration of echo separation for orthogonal waveform encoding mimo-sar based on airborne experiments," *IEEE Transactions on Geoscience and Remote Sensing*, vol. 60, pp. 1–16, 2022.

[4] Y. Cai, Y. Deng, H. Zhang, R. Wang, Y. Wu, and S. Cheng, "An image-domain least L1-Norm method for channel error effect analysis and calibration of azimuth multi-channel SAR," *IEEE Transactions on Geoscience and Remote Sensing*, vol. 60, pp. 1–14, 2022.

[5] A. Moreira, G. Krieger, I. Hajnsek, K. Papathanassiou, M. Younis, P. Lopez-Dekker, S. Huber, M. Villano, M. Pardini, M. Eineder, F. De Zan, and A. Parizzi, "Tandem-L: A highly innovative bistatic SAR mission for global observation of dynamic processes on the earth's surface," *IEEE Geoscience and Remote Sensing Magazine*, vol. 3, no. 2, pp. 8–23, 2015.

[6] Y. Zhang, S. Chang, R. Wang, and Y. Deng, "An innovative push-to-talk (ptt) synchronization scheme for distributed sar," *IEEE Transactions on Geoscience and Remote Sensing*, vol. 60, pp. 1–13, 2022.

[7] Y. Cai, R. Wang, W. Yu, D. Liang, K. Liu, H. Zhang, and Y. Chen, "An advanced approach to improve synchronization phase accuracy with compressive sensing for LT-1 bistatic spaceborne SAR," *Remote Sensing*, vol. 14, no. 18, p. 4621, 2022.

[8] D. Liang, K. Liu, H. Zhang, Y. Chen, H. Yue, D. Liu, Y. Deng, H. Lin, T. Fang, C. Li, and R. Wang, "The processing framework and experimental verification for the noninterrupted synchronization scheme of LuTan-1," *IEEE Transactions on Geoscience and Remote Sensing*, vol. 59, no. 7, pp. 5740–5750, 2021.

[9] G. Jin, K. Liu, D. Liu, D. Liang, H. Zhang, N. Ou, Y. Zhang, Y. Deng, C. Li, and R. Wang, "An advanced phase synchronization scheme for LT-1," *IEEE Transactions on Geoscience and Remote Sensing*, vol. 58, no. 3, pp. 1735–1746, 2020.

[10] Y. Zhang, H. Zhang, N. Ou, K. Liu, D. Liang, Y. Deng, and R. Wang, "First demonstration of multipath effects on phase synchronization scheme for lt-1," *IEEE Transactions on Geoscience and Remote Sensing*, vol. 58, no. 4, pp. 2590–2604, 2020.

[11] D. Liang, H. Zhang, K. Liu, D. Liu, and R. Wang, "Phase synchronization techniques for bistatic and multistatic synthetic aperture radar: Accounting for frequency offset," *IEEE Geoscience and Remote Sensing Magazine*, vol. 10, no. 3, pp. 153–167, 2022.

[12] Y. Zhang, H. Zhang, S. Hou, Y. Deng, W. Yu, and R. Wang, "An innovative superpolyhedron (sp) formation for multistatic sar (m-sar) interferometry," *IEEE Transactions on Geoscience and Remote Sensing*, vol. 59, no. 12, pp. 10 136–10 150, 2021.

[13] Y. Cai, J. Li, Q. Yang, D. Liang, K. Liu, H. Zhang, P. Lu, and R. Wang, "First demonstration of rfi mitigation in the phase synchronization of lt-1 bistatic sar," *IEEE Transactions on Geoscience and Remote Sensing*, pp. 1–1, 2023.

[14] M. Tao, J. Su, Y. Huang, and L. Wang, "Mitigation of radio frequency interference in synthetic aperture radar data: Current status and future trends," *Remote Sensing*, vol. 11, no. 20, p. 2438, 2019.

[15] Y. Huang, G. Liao, J. Li, and J. Xu, "Narrowband RFI suppression for SAR system via fast implementation of joint sparsity and low-rank property," *IEEE Transactions on Geoscience and Remote Sensing*, vol. 56, no. 5, pp. 2748–2761, 2018.

[16] N. Li, Z. Lv, and Z. Guo, "Pulse rfi mitigation in synthetic aperture radar data via a three-step approach: Location, notch, and recovery," *IEEE Transactions on Geoscience and Remote Sensing*, vol. 60, pp. 1–17, 2022.

[17] ——, "Observation and mitigation of mutual rfi between sar satellites: A case study between chinese gaofen-3 and european sentinel-1a," *IEEE Transactions on Geoscience and Remote Sensing*, vol. 60, pp. 1–19, 2022.

[18] V. T. Vu, T. K. Sjögren, M. I. Pettersson, L. Håkansson, A. Gustavsson, and L. M. H. Ulander, "Rfi suppression in ultrawideband sar using an adaptive line enhancer," *IEEE Geoscience and Remote Sensing Letters*, vol. 7, no. 4, pp. 694–698, 2010.

[19] R. Lord and M. Inggs, "Efficient rfi suppression in sar using a lms adaptive filter with sidelobe suppression integrated with the range-doppler algorithm," in *IEEE 1999 International Geoscience and Remote Sensing Symposium. IGARSS'99 (Cat. No.99CH36293)*, vol. 1, 1999, pp. 574–576 vol.1.

[20] F. J. Meyer, J. B. Nicoll, and A. P. Doulgeris, "Correction and characterization of radio frequency interference signatures in l-band synthetic aperture radar data," *IEEE Transactions on Geoscience and Remote Sensing*, vol. 51, no. 10, pp. 4961–4972, 2013.

[21] F. Zhou, R. Wu, M. Xing, and Z. Bao, "Eigensubspace-based filtering with application in narrow-band interference suppression for sar," *IEEE Geoscience and Remote Sensing Letters*, vol. 4, no. 1, pp. 75–79, 2007.

[22] H. Yang, C. Chen, S. Chen, F. Xi, and Z. Liu, "A dictionary-based sar rfi suppression method via robust pca and chirp scaling algorithm," *IEEE Geoscience and Remote Sensing Letters*, vol. 18, no. 7, pp. 1229–1233, 2021.

[23] J. Su, H. Tao, M. Tao, L. Wang, and J. Xie, "Narrow-band interference suppression via rpca-based signal separation in time–frequency domain," *IEEE Journal of Selected Topics in Applied Earth Observations and Remote Sensing*, vol. 10, no. 11, pp. 5016–5025, 2017.

[24] D. Liang, H. Zhang, Y. Cai, K. Liu, and K. Zhang, "An advanced phase synchronization scheme based on coherent integration and waveform diversity for bistatic SAR," *Remote Sensing*, vol. 13, no. 5, p. 981, 2021.

[25] G. Krieger and M. Younis, "Impact of oscillator noise in bistatic and multistatic sar," *IEEE Geoscience and Remote Sensing Letters*, vol. 3, no. 3, pp. 424–428, 2006.

[26] J. Rutman, "Characterization of phase and frequency instabilities in precision frequency sources: Fifteen years of progress," *Proceedings of the IEEE*, vol. 66, no. 9, pp. 1048–1075, 1978.

[27] H. Zhang, W. He, L. Zhang, H. Shen, and Q. Yuan, "Hyperspectral image restoration using low-rank matrix recovery," *IEEE Transactions on Geoscience and Remote Sensing*, vol. 52, no. 8, pp. 4729–4743, 2014.

[28] H. Yang, P. Lang, X. Lu, S. Chen, F. Xi, Z. Liu, and J. Yang, "Robust block subspace filtering for efficient removal of radio interference in synthetic aperture radar images," *IEEE Transactions on Geoscience and Remote Sensing*, vol. 62, pp. 1–12, 2024.

[29] Y. Zhang, B. Du, L. Zhang, and S. Wang, "A low-rank and sparse matrix decomposition-based mahalanobis distance method for hyperspectral anomaly detection," *IEEE Transactions on Geoscience and Remote Sensing*, vol. 54, no. 3, pp. 1376–1389, 2016.

[30] Y. Huang, C. Wen, Z. Chen, J. Chen, Y. Liu, J. Li, and W. Hong, "Hrws sar narrowband interference mitigation using low-rank recovery and image-domain sparse regularization," *IEEE Transactions on Geoscience and Remote Sensing*, vol. 60, pp. 1–14, 2022.

[31] H. Yang, Y. He, Y. Du, T. Zhang, J. Yin, and J. Yang, "Two-dimensional spectral analysis filter for removal of lfm radar interference in space-borne sar imagery," *IEEE Transactions on Geoscience and Remote Sensing*, vol. 60, pp. 1–16, 2022.